Dual Enhancement of Thermostability and Activity of Xylanase through Computer-Aided Rational Design

Meizi Lu,[a,b] Zhihong Li,[b] Hui Zhuang,[b] Shuanghao Yang,[b] Xingchu Zhao,[a] Ruirui Feng,[b] Haoyu Shen,[c] Andrey Kovalevsky,[d] Shengkai Zhang,[e] Zaipeng Xie,[f] Xin Li,[c] Qirong Shen,[a] Qun Wan[a]*

[a] Jiangsu Provincial Key Lab for Solid Organic Waste Utilization, Key lab of organic-based fertilizers of China, Jiangsu Collaborative Innovation Center for Solid Organic Wastes, Educational Ministry Engineering Center of Resource-saving fertilizers, Nanjing Agricultural University, Nanjing 210095, China

[b] College of Science, Nanjing Agricultural University, Nanjing 210095, China

[c] CAS Key Laboratory of Computational Biology, Shanghai Institute of Nutrition and Health, University of Chinese Academy of Sciences, Chinese Academy of Sciences, Shanghai 200031, China

[d] Neutron Scattering Division, Oak Ridge National Laboratory, Oak Ridge, Tennessee 37831, United States of America

[e] Institute of Advanced Science Facilities, Shenzhen 518107, China

[f] Key Laboratory of Water Big Data Technology of Ministry of Water Resources, Hohai University, Nanjing 211100, China

* Corresponding author: qunwan@njau.edu.cn

ABSTRACT

In the realm of enzyme engineering, dual enhancement of thermostability and activity remains a challenge. Herein, we employed a computer-aided approach integrating folding free energy calculations and evolutionary analysis to engineer *Paecilomyces thermophila* xylanase into a hyper-thermophilic enzyme for application in the paper and pulp industry. Through the computational rational design, XynM9 with superior thermostability and enhanced activity was designed. Its optimal reaction temperature increases by 10 °C to 85 °C, its T_m increases by 10 °C to 93 °C, and its half-life increases 11-fold to 5.8 h. Additionally, its catalytic efficiency improves by 57% to 3926 s^{-1} mM^{-1}. Molecular dynamics simulations revealed that XynM9 is stabilized by more hydrogen bonds and salt bridges than the wild-type xylanase. The mutant's narrower catalytic cleft enhances the substrate binding affinity, thus improving the catalytic efficiency. In harsh conditions at 80 °C and pH 10, using XynM9 significantly reduced both hemicellulose and lignin, which makes it a good candidate for use in the paper and pulp process. Our study presents an accurate and efficient strategy for the dual enhancement of enzyme properties, guiding further improvement of computational tools for protein stabilization.

KEYWORDS: xylanase, thermostability, rational design, conservation analysis, folding free energy change

INTRODUCTION

Lignocellulose is the most abundant renewable biomass in nature, composed mainly of cellulose (30-50%), hemicellulose (20-35%), and lignin (10-30%).[1] Endo-1,4-xylanases (EC 3.2.1.8) play a crucial role in the paper and pulp industry by hydrolyzing the hemicellulose backbone.[2] Xylanases from the glycoside hydrolase family 11 (GH11) cleave the β-1,4-xylosidic bonds in xylan through a double-displacement mechanism.[3] This process involves two conserved glutamate residues: one acts as a nucleophile/base, forming a covalent glycosyl-enzyme intermediate while the other functions as a general acid, donating a proton to facilitate glycosidic bond cleavage and stabilize the transition state during catalysis.

Conventional bleaching processes in the paper industry often rely on large quantities of chlorine-based chemicals, which are environmentally hazardous.[4] Utilizing xylanases under alkaline (pH >10) and high-temperature (80~90 °C) conditions can effectively remove both hemicellulose and lignin, thereby increasing cellulose content.[5] However, xylanase activity significantly diminishes under such harsh conditions, limiting their industrial application.[6] XynA from *Paecilomyces thermophila* has a broad pH activity profile at 65 °C, making it a potential candidate for the paper industry.[7] Introducing a disulfide bond in the C-terminal region (XynM2) has elevated its optimal reaction temperature to 75 °C.[8] Nonetheless, its activity significantly dwindles above 80 °C, indicating the need for further improvement.

Directed evolution and rational design are commonly employed strategies for improving enzyme thermostability.[9-11] Directed evolution typically involves too many inferior mutants, necessitating high-throughput screening capabilities.[9, 12] Rational design demands an in-depth understanding of protein structure and function relationships at the atomic level.[11] Modern computer-aided rational design significantly reduces the size of the mutant library and improves protein modification efficiency through techniques such as 3D-structure prediction,[13] folding free energy change ($\Delta\Delta G_{fold}$) calculation,[14] multiple sequence alignment (MSA),[15] and molecular dynamics (MD) simulations[16].

Mutational effects are often quantified by folding free energy change ($\Delta\Delta G_{fold}$), with negative $\Delta\Delta G_{fold}$ values indicating stabilizing mutations and positive $\Delta\Delta G_{fold}$ values suggesting destabilizing mutations.[14] Rosetta[17, 18] and FoldX[19] are effective in calculating $\Delta\Delta G_{fold}$ after mutation.[20] For instance, Zhao et al. employed Rosetta and FoldX to design a stabilizing mutation (D260V) of Proteinase K, resulting in a 12-fold increase of half-life at 69 °C.[21] Chen et al. designed eight stabilizing mutations for Ketoreductase, with three predicted by FoldX and five by Rosetta.[22]

Enzyme dynamics is critical for catalysis.[23] Introducing stabilizing mutations could sometimes jeopardize enzyme dynamics, leading to decreased activity.[24] Therefore, simultaneously improving both thermostability and activity is essential and challenging. Damborky's work strongly suggested that energetic calculations should be complemented by phylogenetic analysis in protein-stabilization endeavors because

more than half (53%) of evolution-based stabilizing mutations would be evaluated as destabilizing by energy calculations.[25] During natural evolution, residues critical for enzyme folding and activity tend to be highly conserved.[26] We believe that mutations with negative $\Delta\Delta G_{fold}$ values and high conservation can improve both thermostability and activity.

There are computational tools and strategies, such as HotSpot Wizard[27] and FireProt,[28] that incorporate both evolutionary-based and energy-based approaches to design single-point and multiple-point stabilizing mutants, respectively. These methods employ FoldX calculations before Rosetta_ddg calculations (or just FoldX) to predict the $\Delta\Delta G_{fold}$ of mutants.[28] FoldX offers faster calculation times, while Rosetta provides increased accuracy.[19] We chose Rosetta Cartesian_ddg,[17] Rosetta ddg_monomer,[29] and FoldX[18] to ensure good coverage of beneficial mutations because their predictions overlapped only in 12%, 15%, or 25%, respectively.[30]

In our study, we combined energy-based and evolution-based analyses to design beneficial mutations of *Paecilomyces thermophila* xylanase (XynM2). Initially, we calculated the $\Delta\Delta G_{fold}$ values for each possible mutation at all residue positions (a total of 3686) using three computational tools (Rosetta Cartesian_ddg, Rosetta ddg_monomer, and FoldX). We then applied multiple sequence alignment to analyze the conservation of these mutations. This process led to the design of eighteen candidate mutations, of which eight were confirmed as beneficial. Finally, we calculated $\Delta\Delta G_{fold}$ for all 440 possible combinations to identify the best combination,

XynM9, which contains seven mutations. This hyper-thermophilic xylanase shows a 10 °C increase in optimal reaction temperature to 85 °C, a 10 °C increase in T_m to 93 °C and an 11-fold extension in half-life to 5.8 h. In addition, its catalytic efficiency improved by 57% compared to XynM2. Under harsh conditions of pH 10 and 80 °C, XynM9 significantly removed both lignin and hemicellulose, increasing cellulose content to 45.9%. This robust and active xylanase has great potential for application in the paper and pulp industry.

RESULTS

Computer-Aided Rational Design

A reliable three-dimensional (3D) structure of an enzyme is essential for rational design of mutations.[31] Among all resolved xylanase crystal structures, the xylanase from *Thermomyces lanuginosus* (PDB ID:1YNA) has the highest sequence identity (94.82%) with XynM2.[32] We built a high-quality 3D model of XynM2 using AlphaFold2 (AF2),[33] and checked its quality using the Ramachandran plot generated by PROCHECK.[34] It shows that 91.8% of residues are located in the most favored regions, 8.2% in allowed regions, and no residues in disallowed regions (Figure S1). Generally, a high-quality model is expected to have over 90% residues in the most favored regions.[35] Molprobity[36] analysis shows that all C_β atoms are positioned within 0.25Å deviation from their ideal values, all bond length deviations are less than 4σ from the ideal values, and no atom clashes are located in the selected regions (Table S1). These results confirm the high quality of the 3D model for rational design.

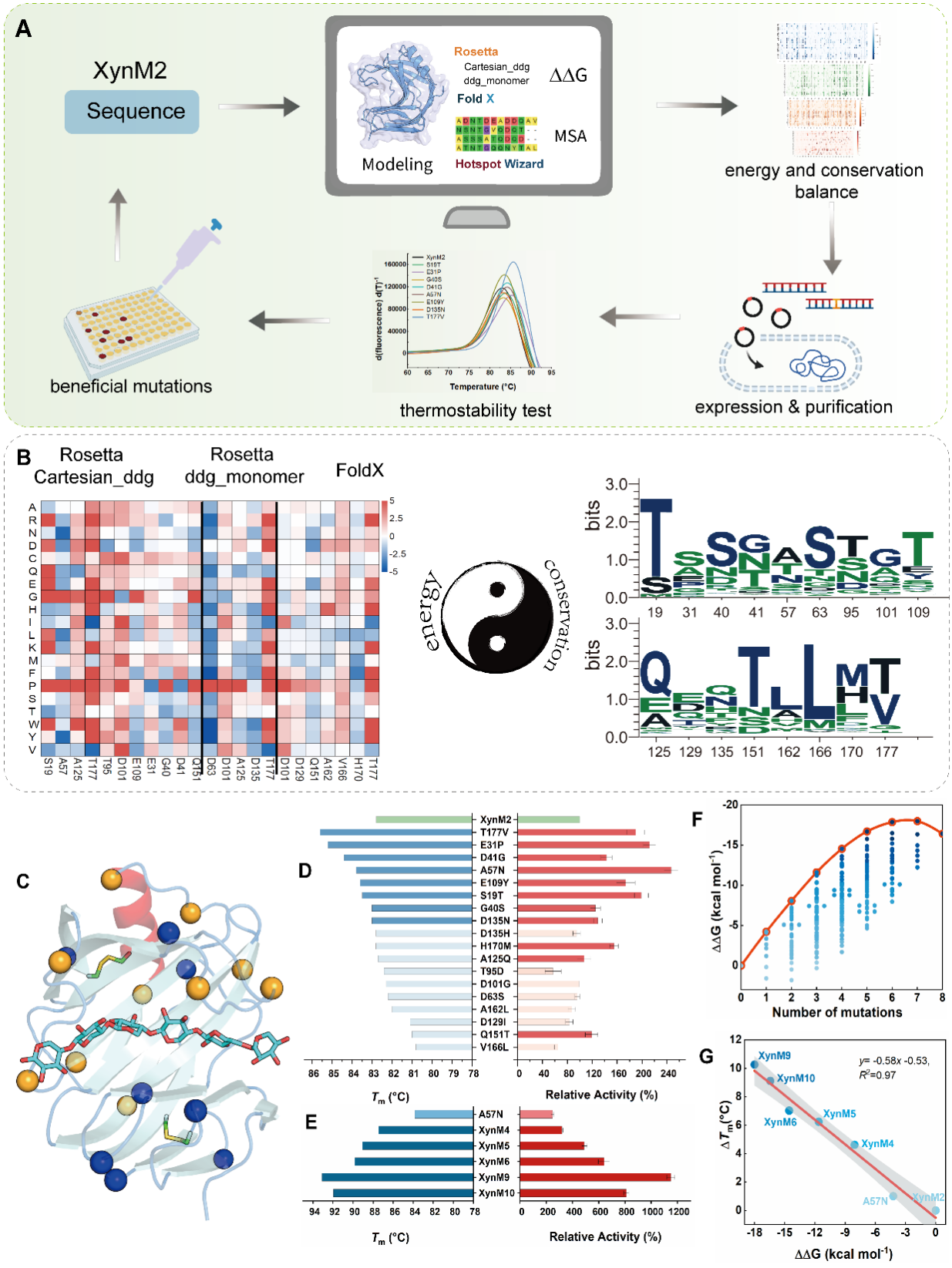

Figure 1. Designing beneficial mutations by $\Delta\Delta G_{fold}$ calculation and conservation analysis. (A) The flow chart of designing and verification. (B) Balancing energy and

conservation according to the Yin-and-Yang theory. $\Delta\Delta G_{fold}$ calculation of all possible mutations using Rosetta Cartesian_ddg, Rosetta ddg_monomer, and FoldX, respectively. Mutations with negative $\Delta\Delta G_{fold}$ values are represented in various shades of blue and mutations with positive $\Delta\Delta G_{fold}$ values are depicted in different shades of red. The frequencies of potential mutations are illustrated by WebLogo. (C) The locations of the eighteen potential mutations are displayed on the modeled structure of XynM2. The Cα atoms of these mutations are depicted as spheres. mutations with higher T_m values, blue; mutations with lower T_m values, orange. Xylohexaose (X6) is a substrate analogue used in crystallization studies to mimic the natural substrate of GH11 xylanases. The structure of X6 was derived from the complex structure of xylanase (PDB ID: 4HK8)[3] and docked into the modeled structure of XynM2. (D) The thermostabilities and relative activities of the potential mutations. (E) The thermostabilities and relative activities of different combinations of mutations. The relative activity was measured at 85 °C for 1 h. the mutants with higher T_m than WT, dark blue; the mutants with lower T_m than WT, light blue; the mutants with higher relative activities, dark red; the mutants with lower relative activities, light red. (F) The minimal $\Delta\Delta G_{fold}$ values for different numbers of combinations are fitted to a parabola curve. The $\Delta\Delta G_{fold}$ values of all combined variants were calculated using Rosetta Cartesian_ddg. The lowest $\Delta\Delta G_{fold}$ values are highlighted in red circles. (G) Correlation between the experimentally measured ΔT_{m} and the calculated $\Delta\Delta G_{fold}$ for XynM2 and the combined mutants. The linear

regression equation is y=-0.58x-0.53, with an R^2 value of 0.97.

Table 1. Rational design based on combination of sequence conservation and $\Delta\Delta G_{fold}$ calculation using different algorithms.

Algorithm	Criteria	Residue	$Frequency_{wt}$ (%)	Mutant	$\Delta\Delta G_{fold}$ (kcal·mol^{-1})	$Frequency_{mut}$ (%)
Rosetta Cartesian_ddg	$\Delta\Delta G_{fold}$ < -2.0 kcal·mol^{-1}, $Frequency_{mut}$ > 10%	S19	2.5	T	-2.64	11.5
		A57	18.0	N	-4.22	11.5
		A125	16.0	Q	-2.75	53.0
		T177	20.5	V	-4.10	17.5
		T95	34.0	D	-2.48	10.5
		D101	5.5	G	-2.45	33.5
		E109	10.5	Y	-2.15	6.5
	$\Delta\Delta G_{fold}$ < -2.0 kcal·mol^{-1}, $Frequency_{mut}$ > $Frequency_{WT}$	E31	2.0	P	-3.35	3.0
	$\Delta\Delta G_{fold}$ < 0 kcal·mol^{-1}, $Frequency_{mut}$ is the highest	G40	0.5	S	-1.19	20.0
		D41	1.5	G	-0.18	10.0
		Q151	0.5	T	-1.16	35
Rosetta ddg_monomer	$\Delta\Delta G_{fold}$ < -2.0 kcal·mol^{-1}, Frequency > 10%	D63	3.5	S	-2.63	37.0
		D101	5.5	G	-2.08	33.5
		A125	16.0	Q	-2.24	53.0
		D135	5.5	H	-2.56	12.0
		D135	5.5	N	-2.02	18.5
		T177	20.5	V	-4.03	17.5
FoldX	$\Delta\Delta G_{fold}$ < -1.0 kcal·mol^{-1}, Frequency > 10%	D101	5.5	G	-1.11	33.5
		D129	19.0	I	-1.42	14.5
		Q151	0.5	T	-1.65	35.0
		A162	8.0	L	-1.22	22.0
		V166	1.0	L	-1.88	37.5
		H170	10.5	M	-2.61	14.0
		T177	20.5	V	-1.97	17.5

We calculated the $\Delta\Delta G_{fold}$ values of all possible mutations at each residue position of XynM2 using three computational tools: Rosetta Cartesian_ddg, Rosetta

ddg_monomer, and FoldX. Each position in XynM2 was individually substituted with the other nineteen natural amino acids, creating three virtual mutant libraries containing 3686 mutations (Figure S2). Lower $\Delta\Delta G_{fold}$ values indicate higher thermostability. However, higher thermostability does not mean higher activity. There are some mutations that result in higher T_m but lower relative activity than that of WT (Table S2). To maintain both high activity and thermostability, we further analyzed the frequency of each mutation using the HotSpot Wizard (Figure S3).[27] Finally, we selected eighteen candidate mutations based on both $\Delta\Delta G_{fold}$ values and amino acid conservation (Figure 1A~B and Table 1): Using Rosetta Cartesian_ddg, we identified seven mutants (S19T, A57N, A125Q, T177V, T95D, D101G, E109Y) whose $\Delta\Delta G_{fold}$ values are less than -2 kcal mol^{-1} and frequencies are above 10%. We also selected one more mutant (E31P) because its $\Delta\Delta G_{fold}$ is -3.35 kcal mol^{-1} and the mutation frequency (3%) is higher than that of WT (2%). Three other mutants (G40S, D41G, Q151T) were selected because their mutation frequencies are the highest even though their $\Delta\Delta G_{fold}$ is just below 0 kcal mol^{-1}. Similarly, we selected six mutants (D63S, D101G, A125Q, D135H, D135N, T177V) based on the Rosetta ddg_monomer calculated $\Delta\Delta G_{fold}$ values (<-2 kcal mol^{-1}) and the sequence conservation (frequency >10%). We also chose seven mutants (D101G, D129I, Q151T, A162L, V166L, H170M, T177V) with the FoldX calculated $\Delta\Delta G_{fold}$ values < -1.0 kcal mol^{-1}) and their sequence conservation (frequencies above 10%). The positions of these mutations are depicted as spheres on the 3D structure of XynM2 (Figure 1C).

Table 2. Activity and thermostability analysis of XynM2 and its mutations.

mutant	Algorithms	T_m (°C)	ΔT_m (°C)	relative activity [a] (%)	T_{opt} (°C)	specific activity [b] (U mg^{-1})	$t_{1/2}^{80}$ [c] (min)
XynM2	-	82.8	0	100	75	12614±95	41
S19T	Rosetta Cartesian_ddg	83.5	0.7	199±11	75	14789±120	44
E31P	Rosetta Cartesian_ddg	85.2	2.4	212±10	80	11540±89	74
G40S	Rosetta Cartesian_ddg	83.0	0.2	125±8	80	11880±96	84
D41G	Rosetta Cartesian_ddg	84.4	1.6	143±9	80	10034±85	74
A57N	Rosetta Cartesian_ddg	83.8	1.0	247±11	80	13873±112	72
E109Y	Rosetta Cartesian_ddg	83.6	0.8	174±15	80	11633±92	58
D135N	Rosetta ddg_Monomer	83.0	0.2	129±7	75	13010±113	55
T177V	Cartesian/Monomer/FoldX	85.6	2.8	190±14	80	12177±95	109

[a] Relative Activities were measured at 85 ° C for an hour to assess the combined effect of activity and stability.

[b] Specific Activities were measured at their optimal reaction temperature for 5 min.

[c] Half-lives of XynM2 and its mutants were measured at 80 °C.

We evaluated the thermostability of XynM2 and its mutants by measuring their melting temperatures (T_m). Out of the eighteen candidates, eight mutants (T177V, E31P, D41G, A57N, E109Y, S19T, G40S, and D135N) have increased T_m values (Figure 1D and Table S3). Notably, T177V and E31P show the most significant increases, reaching 85.6 °C and 85.2°C, respectively. In contrast, the other eleven candidates have lower T_m than XynM2 (Table S3). We also measured the half-lives ($t_{1/2}$) of the eight mutants with higher T_m. All eight mutants (T177V, G40S, D41G, E31P, A57N, E109Y, D135N, and S19T) have higher $t_{1/2}$ of 109, 84, 74, 74, 72, 58, 55, and 44 minutes at 80 °C, respectively (Table 2). However, the increment amplitude of $t_{1/2}$ is inconsistent with that of T_m. For instance, while the ΔT_m of D135N is 0.2 °C, its $t_{1/2}$ increases from 41 to 55 min. Conversely, the ΔT_m of E31P is 2.4 °C,

but its $t_{1/2}$ also increases from 41 to 74 min (Table 2). In addition, six of the eight mutations (excluding S19T and D135N) show an optimal reaction temperature (T_{opt}) of 80 °C, which is 5 °C higher than that of WT (Table 2).

We assessed the relative activities of the eighteen candidates at 85 °C for 1 h to evaluate the combined effect on activity and stability. Among them, eleven mutants (S19T, E31P, G40S, D41G, A57N, E109Y, A125Q, D135N, Q151T, H170M, and T177V) show higher relative activities than that of WT. Particularly, A57N has the most significant increase (247% increased relative activity) (Table 2 and Figure 1D). Interestingly, three mutants (A125Q, Q151T, H170M) with decreased T_m have higher relative activities. We then measured the specific activity of the eight mutants with increased T_m. Among these mutants, three (S19T, A57N, and D135N) have higher specific activity, while the remaining five (T177V, E109Y, E31P, G40S, and D41G) have marginally lower specific activity (Table 2).

Overall, eight mutants among the eighteen candidates simultaneously show increased T_m, $t_{1/2}^{80}$, and relative activities. Rosetta Cartesian_ddg, Rosetta ddg_monomer, and FoldX have successfully predicted seven, two, and one beneficial mutation, respectively. Notably, T177V was predicted as a stable mutation by all three algorithms (Table 1).

Designing the Beneficial Variant XynM9 by Rational Combination

Combining individual stabilizing mutations can largely enhance enzyme stability.[37] We randomly recombined the eight mutations with higher T_m and relative activity and

generated a library containing 247 mutants. Based on our previous findings, Rosetta Cartesian_ddg has the highest accuracy in predicting beneficial mutations. Therefore, we employed Rosetta Cartesian_ddg to calculate the $\Delta\Delta G_{fold}$ values of all combinations. We observed that the minimal $\Delta\Delta G_{fold}$ values for different combinations fit a parabolic curve (Figure 1F). Typically, combining more mutations results in lower minimal $\Delta\Delta G_{fold}$ values. However, the lowest $\Delta\Delta G_{fold}$ value belongs to the variant XynM9 containing seven mutations (S19T/E31P/G40S/D41G/ A57N/E109Y/T177V), whose $\Delta\Delta G_{fold}$ value is -17 kcal mol^{-1}. In comparison, the variant combining all eight mutations (XynM10) has the $\Delta\Delta G_{fold}$ value of -16.43, which is 0.57 higher than XynM9 (Table S4).

To verify whether the calculated $\Delta\Delta G_{fold}$ value can guide the optimal combination, we measured T_m of variants with different combinations with their corresponding minimal $\Delta\Delta G_{fold}$ values (Table S4). We observed that XynM9 has the highest T_m and the lowest $\Delta\Delta G_{fold}$. However, incorporating more mutations does not necessarily incur higher T_m as XynM10 has lower T_m than XynM9. The $\Delta\Delta G_{fold}$ and ΔT_{m} of variants show a strong negative correlation y=-0.58x-0.53 (R^2=0.97) (Figure 1G), indicating that variants with lower calculated $\Delta\Delta G_{fold}$ values are more likely to have higher thermostability (T_m). Among all the combined variants, XynM9 has the highest relative activity (11.5-fold as XynM2) and thermostability (Figure 1E and Table 3). Its T_m is 93.1°C (Table 3), which is 10.3 °C higher than that of XynM2. Its optimal reaction temperature is 85 °C (Figure 3D), which is 10 °C higher than XynM2. Its

half-life at 85 °C is 350 min, which is 11-fold longer than XynM2. Additionally, its catalytic efficiency (k_{cat}/K_m) is 3926s^{-1} mM^{-1} (Table 3), which is 57% higher than that of XynM2.

Table 3. Comparison of kinetics and thermostability between XynM2 and XynM9.

variant	T_m (°C)	relative activity [a] (%)	$t_{1/2}^{85}$ [b] (min)	T_{opt} (°C)	K_m (mM)	k_{cat} (s^{-1})	k_{cat}/K_m (s^{-1} mM^{-1})
XynM2	82.8	100	32	75	2.4±0.1	6002±11	2501
XynM9	93.1	1150±30	350	85	0.7±0.3	2748±24	3926

[a, b] Relative activity and half-lives of XynM2 and XynM9 were measured at 85 °C.

Structure Comparison between XynM9 and XynM2 by Molecular Dynamics Simulation

To elucidate the mechanism behind the thermostability enhancement of XynM9, we performed molecular dynamics (MD) simulations to compare it with XynM2. The MD simulations were executed for 200 ns at 353 K using structures modeled by AF2. The root mean square deviation (RMSD) of these structures reached equilibration after 50 ns (Figure S4). The root mean square fluctuation (RMSF) after equilibration was measured to reflect the mobility of amino acid residues.[38] XynM9 exhibits lower fluctuations in four distinct regions compared to XynM2 : The N-terminal region (from Gln1 to Asn5); the region 1 (from Gly50 to Tyr73, including finger4); the cord region (from Thr 95 to Ala102); the region 2 (from Tyr137 to Asn165, including Helix) (Figure S5 and Figure 2A~B). Reduced fluctuations in these areas suggest that XynM9 has greater stability than XynM2.[38] Interestingly, there are six mutational

positions (19, 31, 40, 41, 109, and 177) located outside these four regions (Figure 2A). This implies that mutations in XynM9 exert a long-distance influence to improve its overall stability.

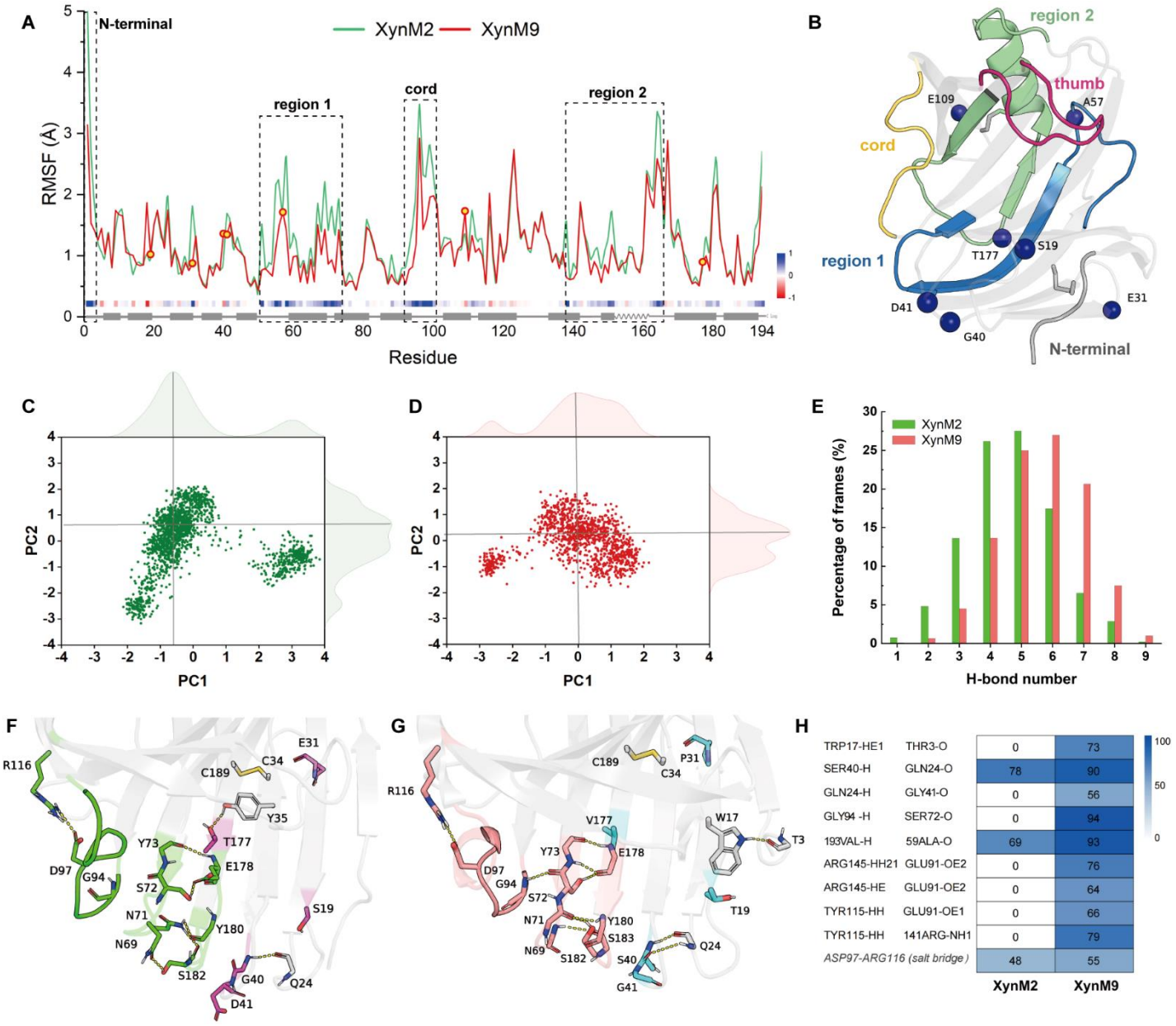

Figure 2. Comparison between XynM2 and XynM9 using MD simulations. (A) RMSF comparison between XynM9 and XynM2 and the significant variations are highlighted in the heat map. the regions with higher RMSF, red; the regions with lower RMSF, blue. Mutational sites are illustrated with circles. (B) The regions with

significant RMSF differences between XynM9 and XynM2 are differentially colored. the N-terminal region (from Gln1 to Asn5), gray; the region 1 (from Gly50 to Tyr73, including L1, b5 and finger 4), sky blue; the cord region (from Thr95 to Ala102), yellow; the thumb region (from Tyr123 to Thr133), pink; the region 2 (from Tyr137 to Asn165, including B7, L2, b6 and Helix), green. The Cα atoms of the stabilized mutations are depicted as blue spheres. (C) The conformational clustering of XynM2. (D) The conformational clustering of XynM9. PC1 and PC2 represent principal components 1 and 2, respectively. The intersection of gray lines indicates the highly aggregated regions of PC1 and PC2. (E) Distribution of H-bonds between Finger 3 and Finger 4. The typical conformations of XynM2 (F) and XynM9 (G). Key residues involved in forming different hydrogen bonds are represented as sticks. The H-bonds are illustrated with yellow dotted lines. (H) Comparison of changes in hydrogen bond occurrence (%) between XynM9 and XynM2 induced by mutations. Hydrogen bonds were evaluated using the geometric cut-off of 3.5 Å for distance and 30° for angle.[39] H-bonds with an occurrence greater than 50% during the simulation were included in the analysis,[40] while those with an occurrence lower than 50% were marked as 0. Only stable salt bridges with an occurrence rate greater than 20% were considered.[22]

Principal Component Analysis (PCA) was employed to compare the major conformation of XynM2 and XynM9.[41] As illustrated in Figure 2C~D, XynM9 exhibits more clustered conformations, with one major and one minor group, whereas XynM2 displays more dispersed conformations, with one major and two minor groups.

We compared the hydrogen bond (H-bond) networks between XynM2 and XynM9 (Figure 2F~G). The mutation T177V disrupts the H-bond between Thr177 and Tyr35. However, this change incurs six H-bonds in XynM9 but only five in XynM2 between Finger 3 and Finger 4 (Figure 2E and S5). There is a new H-bond formed between Gly94 and Ser72 in XynM9 with the probability of 94% (Figure 2H). The probability of salt-bridge formation between Asp97 and Arg116 in XynM9 is 55%, which is 7% higher than in XynM2 (48%). The mutation A57N raises the hydrogen bond probability to 93% between Ala59 and Val193in XynM9, which is 24% higher compared to XynM2 (69%) (Figure 2H). The mutation S19T introduces a new H-bond between Thr3 and Trp17 in XynM9, with the probability of 73%. The mutation E109Y leads to a different H-bond network involving Glu91, Asp111, Gln115, Arg141, and Arg145 in XynM9 (Figure 2H). The mutations G40S and D41G incur an additional H-bond between Finger 1 and 2 in XynM9 compared to XynM2 (Figure 2H and S5). Introducing a proline residue into β-turns (T2) by E31P increases the rigidity of XynM9.[42]

Dynamic Cross-Correlation Matrix (DCCM) reflects the correlation coefficients (C_{ij}) between all pairs of Cα atoms.[43] Overall, XynM9 exhibits similar correlated regions to XynM2 but has fewer anti-correlated regions, suggesting greater stability compared to XynM2 (Figure 3A). Nevertheless, the thumb and finger regions in XynM9 show stronger anti-correlation than those in XynM2, suggesting increased flexibility in this region of XynM9 (Figure 3A). MD trajectories further reveal that the thumb region

and residue Trp18 are more dynamic in XynM9 (Figure 3B). The increased flexibility in the thumb region may facilitate substrate binding to XynM9.[44] The substrate-binding cleft (signified by the distance between the conserved Pro126 and Trp18 residues[44, 45]) in XynM9 is narrower than that in XynM2 (Figure 3C). Additionally, MM/PBSA calculations for the xylanase-xylohexaose complexes reveal that XynM9 has the binding free energy of -47.3 kcal mol^{-1}, which is significantly lower than that of XynM2 (-25.3 kcal mol^{-1}) (Table S5). These results are in agreement with XynM9 having a lower K_m than XynM2 (Table 3).

XynM9 has Higher Activity in the Harsh Condition

We compared the activities between XynM9 and XynM2 under the harsh conditions (80 °C and pH 10). Our results demonstrate that the activity of XynM9 is 3.2-fold higher than that of XynM2. Furthermore, after incubation for 1 h, the residual activity of XynM9 is 4.0-fold higher than that of XynM2 (Figure 3E). Electrostatics analysis shows that the four mutations (E31P, D40S, A57N, and D109Y) increase the positive surface charge of XynM9 (Figure S6).

We compared the hydrolytic effects of wheat straw between XynM2 and XynM9 in the harsh conditions (80 ℃ and pH10) normally employed in the pulp industry. After 24 hours of hydrolysis by XynM9, the pulp quality was significantly improved (Figure 3F): The hemicellulose content decreased from 25.3% to 13.5%, the lignin content decreased from 9.4% to 6.8%, and the cellulose content increased from 32.3% to 45.9%. In contrast, applying XynM2 only marginally improved the pulp quality:

The hemicellulose content slightly decreased from 25.3% to 22.8%, the lignin content slightly decreased from 9.4% to 8.6%, and the cellulose content mildly increased from 32.3% to 35.6%.

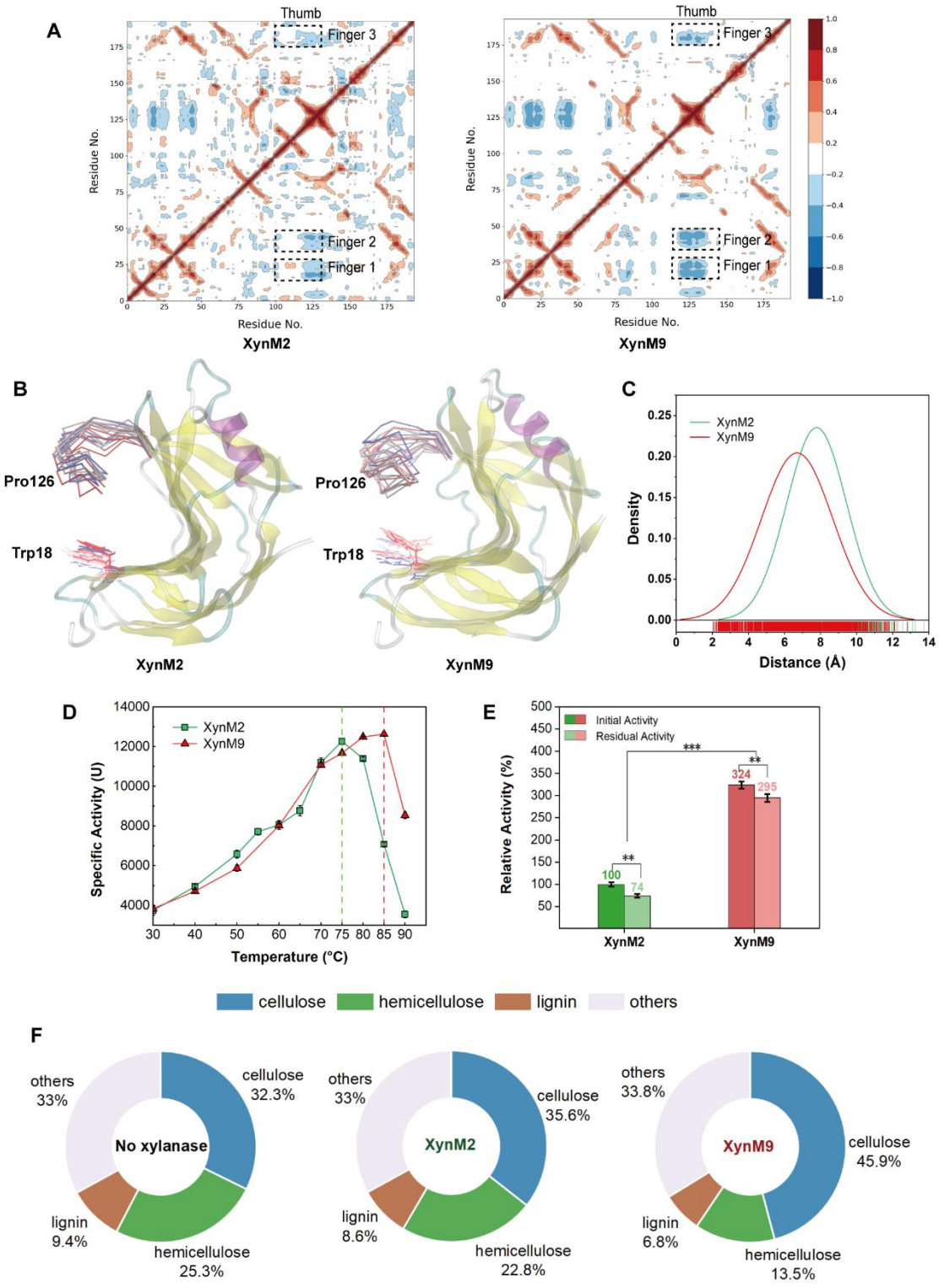

Figure 3. The more closed conformation of XynM9 leads to higher substrate binding affinity and catalytic activity. (A) DCCM differences of the Cα atom pairs between XynM2 and XynM9. The different correlation coefficients (C_{ij}) are color-coded according to the following rules: C_{ij} with values from 0.2 to 1 represents the positive

correlations (red); C_{ij} with values from -1 to -0.2 represents anti-correlation (blue); C_{ij} with values from -0.2 to 0.2 represents weak or no-correlation (white). (B) Comparison of the of the thumb regions dynamics between XynM2 and XynM9. (C) The distance from Trp18 to Pro126 in XynM9 is narrower than that of XynM2 during MD simulations. (D) Comparison of temperature-dependent activity between XynM2 and XynM9 at pH 7.0. (E) Comparison of the activity and stability between XynM2 and XynM9. The activity assay was carried out according to the standard protocol at pH 10 and 80 °C. The dark colors represent the relative activity and the light colors represent the residual activity after incubation for 1 h. (F) XynM9 has significantly better efficacy than XynM2 to remove both hemicellulose and lignin in the harsh conditions (80 °C and pH 10).

DISCUSSION

Xylanase is a key biocatalyst for degrading hemicellulose and has been widely used in the paper and pulp industry. It can improve paper whiteness and reduce the usage of chlorine-based bleaching chemicals.[4] However, xylanase needs to function under the high temperatures and alkaline conditions.[5] Xylanase from *Paecilomyces thermophila* (XynA) has potential to be used in the pulp industry due to its high activity in the alkaline conditions with the optimal temperature at 65 °C. Wu et al. introduced a disulfide bond in its N-terminal region and increased its optimal temperature to 75 °C (XynM2).[8] However, its activity still quickly diminishes in harsh conditions of the pulp industry (80~85°C, pH>10).[7] We aim to further enhance

its longevity using a computer-aided rational strategy, which is based on the balance between folding free energy change ($\Delta\Delta G_{fold}$) and sequence conservation.

Mutants with negative $\Delta\Delta G_{fold}$ values are predicted to have higher thermostability.[46] Different algorithms apply different thresholds for accurate estimation: -2 kcal mol^{-1} for Rosetta and -1 kcal mol^{-1} for FoldX, respectively.[28] However, relying solely on $\Delta\Delta G_{fold}$ is insufficient for designing a robust and active biocatalyst. For instance, S16Y mutant has the calculated $\Delta\Delta G_{fold}$ of -8.8 kcal mol^{-1} and a ΔT_m of 7 °C. Unfortunately, it only maintains less than 3% activity (Table S2). Structure analysis suggests that the Tyr16 side chain blocks the substrate binding pocket, thereby affecting the enzyme's activity (Figure S7). The solely energy-based approach disregards residues critical for enzymatic activity, leading to mutations that increase thermostability but decrease activity. Substitution with highly conserved residues benefits both enzymatic activity and thermostability.[26] Thus, we combined sequence conservation and $\Delta\Delta G_{fold}$ calculation to select potential mutations.

We generated three virtual permutation libraries (including 3686 mutations) based on $\Delta\Delta G_{fold}$ calculations and screened their conservation for selecting beneficial mutations. Using the criteria outlined in Table 1, we proposed eighteen mutations. After experimental testing, eight single mutants demonstrated both higher activity and stability. All mutations with increased thermostability also exhibited higher activity, indicating that our strategy is quite successful (Figure 1D). Using the same frequency threshold (>10%), Rosetta Cartesian_ddg ($\Delta\Delta G_{fold}$ < -2.0 kcal mol^{-1}), Rosetta

ddg_monomer ($\Delta\Delta G_{fold}$ < -2.0 kcal mol^{-1}), and FoldX ($\Delta\Delta G_{fold}$ < -1.0 kcal mol^{-1}) successfully estimated 50%, 33%, and 14% beneficial mutations, individually. The varing accuracy of these algorithms is attributable to their different functions in calculating free energy changes.[28] Rosetta ddg_monomer requires many replicates with strong constraints. In comparison, Rosetta Cartesian_ddg allows small local backbone movements during refinement,[17] which improves the Pearson correlation between the estimated and experimentally measured $\Delta\Delta G_{fold}$ values.[17] Therefore, the Rosetta Cartesian_ddg energy function (opt-nov15)[17] outperforms Rosetta ddg_monomer energy function (talaris2014)[29] in many prediction tests. FoldX has lower accuracy in our case, possibly due to the limitations of backbone stiffness during sampling.[19, 47, 48] We initially identified five beneficial mutations using the recommended criteria, but these were insufficient to meet the thermostability requirement of the paper and pulp industry. Consequently, we adjusted the balance between energy and conservation by applying varied threshold, leading to the identification of four additional candidates (E31P, G40S, D41G, Q151T) (Table 1). Among them, three were experimentally confirmed to be beneficial.

In our approach, we considered both conservation enhancement and energy reduction as criteria, and aimed balance the strictness of these two conditions. When one criterion was applied more rigorously, we could still identify effective mutations by slightly relaxing the other criterion (Table 1 and Figure 1). This trade-off is akin to the Yin and Yang concept in Chinese philosophy, which symbolizes the balance of

complementary forces.[49] In computer-aided enzyme engineering, predictions often include many false negatives and false positives. By adjusting energy and conservation criteria, we were able to reduc these false-negative and false-positive mutations. Consequently, our strategy achieved a high success rate in predictions: out of the eleven candidates proposed by Rosetta Cartesian_ddg, seven were experimentally verified as beneficial mutations (Table 2).

Combining beneficial mutations commonly results in a superior variant.[37] However, simply combining all beneficial mutations (XynM10) does not yield the best performance, although XynM10 still significantly outperforms XynM2 (Figure 1E). By calculating $\Delta\Delta G_{fold}$ for all possible combinations using Rosetta Cartesian_ddg, we found that XynM9 with seven mutations has the lowest calculated ΔG_{fold} (Figure 1F). Compared to XynM2, its optimal reaction temperature increases from 75 °C to 85 °C, its T_m increases from 83 °C to 93 °C, and its half-life extends to 5.8 hours (11-fold) at 85 °C. Moreover, its catalytic efficiency improves by 57%, reaching 3926 s^{-1} mM^{-1} (Table 3). These results indicate that our strategy of computer-aided combination is very helpful in designing the most powerful variant.

XynM9, compared to XynM2, exhibits more stable intramolecular interactions (hydrogen bonds and ionic interactions) in the N-terminal, the region 1, the cord, and the region 2 (Figure 2). MD simulations analysis shows lower RMSF for its catalytic amino acids (Glu86 and Glu178), suggesting dampened dynamics of these key residues (Figure 2A). Dynamics of Glu178 is essential for catalysis as the acid/base.[23]

Thus, k_{cat} for XynM9 is lower than that for XynM2. However, MD analysis reveals a narrower substrate-binding cleft in XynM9 (Figure 3C), which leads to higher substrate binding affinity (K_m decreases from 2.4 to 0.7 mM) (Table 3) and decreased binding free energy (-22 kcal mol^{-1}) (Table S5). As a result, its catalytic efficiency (k_{cat}/K_m) is improved by 57% (Table 3). In addition, four mutations (E31P, D40S, A57N, and D109Y) increase the electrostatic positive charge on the protein surface (Figure S6), potentially increasing alkaline tolerance in GH11 xylanase, aligning with findings from previous studies. [50,51]

Numerous strategies have been successfully employed to design and enhance the thermostability of xylanase.[52-58] For example, introducing disulfide bonds,[53] sandwich fusion with CBM9_2,[54] and targeted modifications of the N-terminus and core regions[55] have significantly increased the melting temperatures of various xylanases, such as DSB1 (74°C), C2-XYN-C2 (53°C), and reATX11A41/cord (72°C). Surface engineering, such as substituting Ser/Thr with Arg or Thr,[57, 58] has also improved thermostability and optimal temperatures (Table S6). These rational design strategies, while requiring relatively minimal effort, have produced xylanase mutants with improved thermostability. However, the thermostability and activity levels remain insufficient for the stringent requirements of the paper industry. In contrast, Wu et al.[52] utilized a combination strategy based on energy calculations and molecular dynamics (MD) simulations. This approach involved screening 105 XynCDBFV mutants and identifying 10 mutations that enhanced thermostability. The combination of these

mutations increased the optimal temperature of XynCDBFV-m to 65°C, with a substantial enzyme activity of 11,000 U mg^{-1}. In our study, we employed a computer-aided approach integrating folding free energy calculations and evolutionary analysis that resulted in the design of XynM9, a mutant that exhibits superior activity and thermostability compared to other reported strategies. XynM9 achieved a melting temperature of 93°C and an enzyme activity of 12,630 U mg^{-1}. It demonstrated exceptional efficacy in removing both hemicellulose and lignin from wheat straw fibers under harsh conditions (80 °C and pH 10), indicating its excellent potential for application in the paper and pulp industry. More importantly, our screening method has been optimized to identify more beneficial mutations with a reasonable experimental workload, thus significantly reducing both effort and cost.

CONCLUSION

By balancing energy and conservation with the Yin-and-Yang theory, we have developed an accurate, cost-effective, and efficient strategy to engineer a hyper-thermophilic and highly active xylanase. It has demonstrated exceptional efficacy in removing hemicellulose and lignin under harsh conditions (80 °C and pH 10), which shows great potential application in the paper and pulp industry. Our integrated strategy provides guidance in enzyme engineering to improve both thermostability and activity.

ASSOCIATED CONTENT

Supporting Information

The Supporting Information is available free of charge via the website. Material and methods, evaluation of the AF2-built model of XynM2 using MolProbity (Table S1), characteristics of mutants with substantially reduced ΔG_{fold} and low frequency (Table S2), the relative activities and thermal stabilities of the proposed mutants (Table S3), calculated $\Delta\Delta G_{fold}$ and characterization of the combined mutants (Table S4), comparing the binding free energy of XynM2-X6 and XynM9-X6 (Table S5), examples of engineering using various strategies (Table S6), primers used in this study (Table S7), Ramachandran plot of the AF2 built model for XynM2 (Figure S1), the $\Delta\Delta G_{fold}$ heatmaps of all possible mutations calculated using Rosetta Cartesian_ddg, Rosetta ddg_monomer, and FoldX (Figure S2), the frequency heatmap of XnyM2 analyzed using the Hotspot Wizard (Figure S3), RMSD analysis for XynM2, XynM9, the XynM2-X6 complex, and the XynM9-X6 complex after MD simulations at 353 K (Figure S4), the built structure of XynM2 (Figure S5), electrostatics comparison between XynM2 and XynM9 (Figure S6), comparison of the substrate-binding pocket between XynM2 and the mutant S16Y (Figure S7), the melt curves of all selected single-point mutants and the combined mutants (Figure S8), the half-lives ($t_{1/2}$) of XynM2 and its mutants at 80 °C and 85 °C (Figure S9), and SDS-PAGE analysis of the purified mutants (Figure S10).

AUTHOR INFORMATION

Corresponding Author

Qun Wan − Jiangsu Provincial Key Lab for Solid Organic Waste Utilization, Key lab of organic-based fertilizers of China, Jiangsu Collaborative Innovation Center for Solid Organic Wastes, Educational Ministry Engineering Center of Resource-saving fertilizers, Nanjing Agricultural University, Nanjing 210095, China

orcid.org/0000-0002-8309-0341; Email: qunwan@ njau.edu.cn

Notes

The authors declare the following competing financial interest (s): We declare that Nanjing Agricultural University has filed a patent for a xylanase designed by the report.

ACKNOWLEDGMENTS

Q.W. was supported by the National Natural Science Foundation of China (no. 32071264 and no. 32271317) and the Jiangsu Collaborative Innovation Center for Solid Organic Waste Resource Utilizationand.

REFERENCES

1. Ajeje, S. B.; Hu, Y.; Song, G.; Peter, S. B.; Afful, R. G.; Sun, F.; Asadollahi, M. A.; Amiri, H.; Abdulkhani, A.; Sun, H., Thermostable Cellulases / Xylanases From Thermophilic and Hyperthermophilic Microorganisms: Current Perspective. *Front Bioeng Biotechnol* **2021,** *9*, 794304.
2. Juturu, V.; Wu, J. C., Microbial xylanases: Engineering, production and industrial applications. *Biotechnology Advances* **2012,** *30* (6), 1219-1227.
3. Wan, Q.; Zhang, Q.; Hamilton-Brehm, S.; Weiss, K.; Mustyakimov, M.; Coates, L.; Langan, P.; Graham, D.; Kovalevsky, A., X-ray crystallographic studies of family 11 xylanase Michaelis and product complexes: implications for the catalytic mechanism. *Acta Crystallogr D Biol Crystallogr* **2014,** *70* (Pt 1), 11-23.
4. Sarma, R. K.; Gohain, A.; Ahmed, T. H.; Yadav, A.; Saikia, R., An environment-benign approach of bamboo pulp bleaching using extracellular xylanase of strain *Bacillus stratosphericus* EB-11 isolated from elephant dung. *Folia Microbiologica* **2023,** *68* (1), 135-149.
5. Techapun, C.; Poosaran, N.; Watanabe, M.; Sasaki, K., Thermostable and alkaline-tolerant microbial cellulase-free xylanases produced from agricultural wastes and the properties required for use in pulp bleaching bioprocesses: a review. *Process Biochemistry* **2003,** *38* (9), 1327-1340.
6. Shah, A. K.; Sidid, S. S.; Ahmad, A.; Rele, M. V., Treatment of bagasse pulp with cellulase-free xylanases from an alkalophilic *Bacillus sp*. Sam-3. *Bioresource Technology* **1999,** *68* (2), 133-140.
7. Zhang, M.; Jiang, Z.; Yang, S.; Hua, C.; Li, L., Cloning and expression of a *Paecilomyces thermophila* xylanase gene in *E. coli* and characterization of the recombinant xylanase. *Bioresour Technol* **2010,** *101* (2), 688-95.
8. Bao, K.; Wu, X.-X. Alkaline xylanase mutant with high specific activity. Patent CN115851668 (A) 2023. 0328.
9. Jaeger, K. E.; Eggert, T., Enantioselective biocatalysis optimized by directed evolution. *Curr Opin Biotechnol* **2004,** *15* (4), 305-13.
10. Acevedo-Rocha, C. G.; Hollmann, F.; Sanchis, J.; Sun, Z., A Pioneering Career in Catalysis: Manfred T. Reetz. *ACS Catalysis* **2020,** *10* (24), 15123-15139.
11. Ni, D.; Zhang, S.; Kırtel, O.; Xu, W.; Chen, Q.; Öner, E. T.; Mu, W., Improving the Thermostability and Catalytic Activity of an Inulosucrase by Rational Engineering for the Biosynthesis of Microbial Inulin. *Journal of Agricultural and Food Chemistry* **2021,** *69* (44), 13125-13134.
12. Reetz, M. T.; Qu, G.; Sun, Z., Engineered enzymes for the synthesis of pharmaceuticals and other high-value products. *Nature Synthesis* **2024,** *3* (1), 19-32.
13. Tunyasuvunakool, K.; Adler, J.; Wu, Z.; Green, T.; Zielinski, M.; Zidek, A.; Bridgland, A.; Cowie, A.; Meyer, C.; Laydon, A.; Velankar, S.; Kleywegt, G. J.; Bateman, A.; Evans, R.; Pritzel, A.; Figurnov, M.; Ronneberger, O.; Bates, R.; Kohl, S. A. A.; Potapenko, A.; Ballard, A. J.; Romera-Paredes, B.; Nikolov, S.; Jain, R.; Clancy, E.; Reiman, D.; Petersen, S.; Senior, A. W.; Kavukcuoglu, K.; Birney, E.; Kohli, P.; Jumper, J.; Hassabis, D., Highly accurate protein structure prediction for the human proteome. *Nature* **2021,** *596* (7873), 590-596.
14. Sun, Z.; Liu, Q.; Qu, G.; Feng, Y.; Reetz, M. T., Utility of B-Factors in Protein Science: Interpreting Rigidity, Flexibility, and Internal Motion and Engineering Thermostability. *Chem Rev* **2019,**

119 (3), 1626-1665.

15. Wang, T.; Liang, C.; Hou, Y.; Zheng, M.; Xu, H.; An, Y.; Xiao, S.; Liu, L.; Lian, S., Small design from big alignment: engineering proteins with multiple sequence alignment as the starting point. *Biotechnology Letters* **2020,** *42* (8), 1305-1315.

16. Kutzner, C.; Pall, S.; Fechner, M.; Esztermann, A.; de Groot, B. L.; Grubmuller, H., Best bang for your buck: GPU nodes for GROMACS biomolecular simulations. *J Comput Chem* **2015,** *36* (26), 1990-2008.

17. Park, H.; Bradley, P.; Greisen, P.; Liu, Y.; Mulligan, V. K.; Kim, D. E.; Baker, D.; DiMaio, F., Simultaneous Optimization of Biomolecular Energy Functions on Features from Small Molecules and Macromolecules. *J Chem Theory Comput* **2016,** *12* (12), 6201-6212.

18. Kellogg, E. H.; Leaver-Fay, A.; Baker, D., Role of conformational sampling in computing mutation-induced changes in protein structure and stability. *Proteins* **2011,** *79* (3), 830-8.

19. Buss, O.; Rudat, J.; Ochsenreither, K., FoldX as Protein Engineering Tool: Better Than Random Based Approaches? *Comput Struct Biotechnol J* **2018,** *16*, 25-33.

20. Lutz, S., Beyond directed evolution--semi-rational protein engineering and design. *Curr Opin Biotechnol* **2010,** *21* (6), 734-43.

21. Zhao, Y.; Li, D.; Bai, X.; Luo, M.; Feng, Y.; Zhao, Y.; Ma, F.; Yang, G.-Y., Improved thermostability of proteinase K and recognizing the synergistic effect of Rosetta and FoldX approaches. *Protein Engineering, Design and Selection* **2021,** *34*, gzab024.

22. Chen, C.; Guan, B.-H.; Geng, Q.; Zheng, Y.-C.; Chen, Q.; Pan, J.; Xu, J.-H., Enhanced Thermostability of *Candida* Ketoreductase by Computation-Based Cross-Regional Combinatorial Mutagenesis. *ACS Catalysis* **2023**, 7407-7416.

23. Li, Z.; Zhang, X.; Wang, Q.; Li, C.; Zhang, N.; Zhang, X.; Xu, B.; Ma, B.; Schrader, T. E.; Coates, L.; Kovalevsky, A.; Huang, Y.; Wan, Q., Understanding the pH-Dependent Reaction Mechanism of a Glycoside Hydrolase Using High-Resolution X-ray and Neutron Crystallography. *ACS Catalysis* **2018,** *8* (9), 8058-8069.

24. Beadle, B. M.; Shoichet, B. K., Structural bases of stability-function tradeoffs in enzymes. *Journal of Molecular Biology* **2002,** *321* (2), 285-296.

25. Beerens, K.; Mazurenko, S.; Kunka, A.; Marques, S. M.; Hansen, N.; Musil, M.; Chaloupkova, R.; Waterman, J.; Brezovsky, J.; Bednar, D.; Prokop, Z.; Damborsky, J., Evolutionary Analysis As a Powerful Complement to Energy Calculations for Protein Stabilization. *ACS Catalysis* **2018,** *8* (10), 9420-9428.

26. Lehmann, M.; Pasamontes, L.; Lassen, S. F.; Wyss, M., The consensus concept for thermostability engineering of proteins. *Biochimica et Biophysica Acta (BBA) - Protein Structure and Molecular Enzymology* **2000,** *1543* (2), 408-415.

27. Sumbalova, L.; Stourac, J.; Martinek, T.; Bednar, D.; Damborsky, J., HotSpot Wizard 3.0: web server for automated design of mutations and smart libraries based on sequence input information. *Nucleic Acids Res* **2018,** *46* (W1), W356-W362.

28. Bednar, D.; Beerens, K.; Sebestova, E.; Bendl, J.; Khare, S.; Chaloupkova, R.; Prokop, Z.; Brezovsky, J.; Baker, D.; Damborsky, J., FireProt: Energy- and Evolution-Based Computational Design of Thermostable Multiple-Point Mutants. *PLoS Comput Biol* **2015,** *11* (11), e1004556.

29. O'Meara, M. J.; Leaver-Fay, A.; Tyka, M. D.; Stein, A.; Houlihan, K.; DiMaio, F.;

Bradley, P.; Kortemme, T.; Baker, D.; Snoeyink, J.; Kuhlman, B., Combined covalent-electrostatic model of hydrogen bonding improves structure prediction with Rosetta. *J Chem Theory Comput* **2015,** *11* (2), 609-622.

30. Wijma, H. J.; Floor, R. J.; Jekel, P. A.; Baker, D.; Marrink, S. J.; Janssen, D. B., Computationally designed libraries for rapid enzyme stabilization. *Protein Engineering, Design and Selection* **2014,** *27* (2), 49-58.

31. Rahban, M.; Zolghadri, S.; Salehi, N.; Ahmad, F.; Haertlé, T.; Rezaei-Ghaleh, N.; Sawyer, L.; Saboury, A. A., Thermal stability enhancement: Fundamental concepts of protein engineering strategies to manipulate the flexible structure. *International Journal of Biological Macromolecules* **2022,** *214*, 642-654.

32. Gruber, K.; Klintschar, G.; Hayn, M.; Schlacher, A.; Steiner, W.; Kratky, C., Thermophilic xylanase from *Thermomyces lanuginosus*: high-resolution X-ray structure and modeling studies. *Biochemistry* **1998,** *37* (39), 13475-13485.

33. Jumper, J.; Evans, R.; Pritzel, A.; Green, T.; Figurnov, M.; Ronneberger, O.; Tunyasuvunakool, K.; Bates, R.; Zidek, A.; Potapenko, A.; Bridgland, A.; Meyer, C.; Kohl, S. A. A.; Ballard, A. J.; Cowie, A.; Romera-Paredes, B.; Nikolov, S.; Jain, R.; Adler, J.; Back, T.; Petersen, S.; Reiman, D.; Clancy, E.; Zielinski, M.; Steinegger, M.; Pacholska, M.; Berghammer, T.; Bodenstein, S.; Silver, D.; Vinyals, O.; Senior, A. W.; Kavukcuoglu, K.; Kohli, P.; Hassabis, D., Highly accurate protein structure prediction with AlphaFold. *Nature* **2021,** *596* (7873), 583-589.

34. Laskowski, R. A.; Rullmannn, J. A.; MacArthur, M. W.; Kaptein, R.; Thornton, J. M., AQUA and PROCHECK-NMR: programs for checking the quality of protein structures solved by NMR. *J Biomol NMR* **1996,** *8* (4), 477-486.

35. Rai, D. K.; Rieder, E. Homology Modeling and Analysis of Structure Predictions of the Bovine Rhinitis B Virus RNA Dependent RNA Polymerase (RdRp) *International Journal of Molecular Sciences* [Online], 2012, p. 8998-9013.

36. Williams, C. J.; Headd, J. J.; Moriarty, N. W.; Prisant, M. G.; Videau, L. L.; Deis, L. N.; Verma, V.; Keedy, D. A.; Hintze, B. J.; Chen, V. B.; Jain, S.; Lewis, S. M.; Arendall, W. B.; Snoeyink, J.; Adams, P. D.; Lovell, S. C.; Richardson, J. S.; Richardson, D. C., MolProbity: More and better reference data for improved all-atom structure validation. *Protein Science : a Publication of the Protein Society* **2018,** *27* (1), 293-315.

37. Ahmed, S.; Manjunath, K.; Chattopadhyay, G.; Varadarajan, R., Identification of stabilizing point mutations through mutagenesis of destabilized protein libraries. *J Biol Chem* **2022,** *298* (4), 101785.

38. Berhanu, W. M.; Masunov, A. E., Full length amylin oligomer aggregation: insights from molecular dynamics simulations and implications for design of aggregation inhibitors. *J Biomol Struct Dyn* **2014,** *32* (10), 1651-1669.

39. Luzar, A., Resolving the hydrogen bond dynamics conundrum. *The Journal of Chemical Physics* **2000,** *113* (23), 10663-10675.

40. Blaszczyk, J.; Lu, Z.; Li, Y.; Yan, H.; Ji, X., Crystallographic and molecular dynamics simulation analysis of *Escherichia coli* dihydroneopterin aldolase. *Cell & Bioscience* **2014,** *4* (1), 52.

41. Cui, H.; Eltoukhy, L.; Zhang, L.; Markel, U.; Jaeger, K.-E.; Davari, M. D.; Schwaneberg,

U., Less Unfavorable Salt Bridges on the Enzyme Surface Result in More Organic Cosolvent Resistance. *Angewandte Chemie International Edition* **2021,** *60* (20), 11448-11456.

42. Watanabe, K.; Suzuki, Y., Protein thermostabilization by proline substitutions. *Journal of Molecular Catalysis B: Enzymatic* **1998,** *4* (4), 167-180.

43. Wang, Y.; Ji, D.; Lei, C.; Chen, Y.; Qiu, Y.; Li, X.; Li, M.; Ni, D.; Pu, J.; Zhang, J.; Fu, Q.; Liu, Y.; Lu, S., Mechanistic insights into the effect of phosphorylation on Ras conformational dynamics and its interactions with cell signaling proteins. *Comput Struct Biotechnol J* **2021,** *19*, 1184-1199.

44. Paes, G.; Berrin, J. G.; Beaugrand, J., GH11 xylanases: Structure/function/properties relationships and applications. *Biotechnol Adv* **2012,** *30* (3), 564-92.

45. Paes, G.; Cortes, J.; Simeon, T.; O'Donohue, M. J.; Tran, V., Thumb-loops up for catalysis: a structure/function investigation of a functional loop movement in a GH11 xylanase. *Comput Struct Biotechnol J* **2012,** *1*, e201207001.

46. Szymczyk, P.; Szymańska, G.; Lipert, A.; Weremczuk-Jeżyna, I.; Kochan, E., Computer-Aided Saturation Mutagenesis of *Arabidopsis thaliana* Ent-Copalyl Diphosphate Synthase. *Interdisciplinary Sciences: Computational Life Sciences* **2020,** *12* (1), 32-43.

47. Sora, V.; Laspiur, A. O.; Degn, K.; Arnaudi, M.; Utichi, M.; Beltrame, L.; De Menezes, D.; Orlandi, M.; Stoltze, U. K.; Rigina, O.; Sackett, P. W.; Wadt, K.; Schmiegelow, K.; Tiberti, M.; Papaleo, E., RosettaDDGPrediction for high-throughput mutational scans: From stability to binding. *Protein Sci* **2023,** *32* (1), e4527.

48. Usmanova, D. R.; Bogatyreva, N. S.; Ariño Bernad, J.; Eremina, A. A.; Gorshkova, A. A.; Kanevskiy, G. M.; Lonishin, L. R.; Meister, A. V.; Yakupova, A. G.; Kondrashov, F. A.; Ivankov, D. N., Self-consistency test reveals systematic bias in programs for prediction change of stability upon mutation. *Bioinformatics* **2018,** *34* (21), 3653-3658.

49. Guo-Ming, C., Bian (Change): A Perpetual Discourse of I Ching. *Intercultural Communication Studies* **2008,** *vol. 17,no. 4*, 7-16.

50. Wu, X.; Zhang, Q.; Zhang, L.; Liu, S.; Chen, G.; Zhang, H.; Wang, L., Insights Into the Role of Exposed Surface Charged Residues in the Alkali-Tolerance of GH11 Xylanase. *Front Microbiol* **2020,** *11*, 872.

51. Shirai, T.; Suzuki, A.; Yamane, T.; Ashida, T.; Kobayashi, T.; Hitomi, J.; Ito, S., High-resolution crystal structure of M-protease: phylogeny aided analysis of the high-alkaline adaptation mechanism. *Protein Engineering, Design and Selection* **1997,** *10* (6), 627-634.

52. Bu, Y.; Cui, Y.; Peng, Y.; Hu, M.; Tian, Y.; Tao, Y.; Wu, B., Engineering improved thermostability of the GH11 xylanase from *Neocallimastix patriciarum* via computational library design. *Appl Microbiol Biotechnol* **2018,** *102* (8), 3675-3685.

53. Wang, Y.; Fu, Z.; Huang, H.; Zhang, H.; Yao, B.; Xiong, H.; Turunen, O., Improved thermal performance of *Thermomyces lanuginosus* GH11 xylanase by engineering of an N-terminal disulfide bridge. *Bioresour Technol* **2012,** *112*, 275-9.

54. Yang, A.; Cheng, J.; Liu, M.; Shangguan, Y.; Liu, L., Sandwich fusion of CBM9_2 to enhance xylanase thermostability and activity. *Int J Biol Macromol* **2018,** *117*, 586-591.

55. Li, C.; Li, J.; Wang, R.; Li, X.; Li, J.; Deng, C.; Wu, M., Substituting Both the N-Terminal and "Cord" Regions of a Xylanase from *Aspergillus oryzae* to Improve Its Temperature

Characteristics. *Appl Biochem Biotechnol* **2018,** *185* (4), 1044-1059.
56. Xing, H.; Zou, G.; Liu, C.; Chai, S.; Yan, X.; Li, X.; Liu, R.; Yang, Y.; Zhou, Z., Improving the thermostability of a GH11 xylanase by directed evolution and rational design guided by B-factor analysis. *Enzyme Microb Technol* **2021,** *143*, 109720.
57. Satyanarayana, D. V., Improvement in thermostability of metagenomic GH11 endoxylanase (Mxyl) by site-directed mutagenesis and its applicability in paper pulp bleaching process. *J Ind Microbiol Biotechnol* **2013,** *40* (12), 1373-81.
58. Zouari Ayadi, D.; Hmida Sayari, A.; Ben Hlima, H.; Ben Mabrouk, S.; Mezghani, M.; Bejar, S., Improvement of *Trichoderma reesei* xylanase II thermal stability by serine to threonine surface mutations. *Int J Biol Macromol* **2015,** *72*, 163-70

For Table of Contents Only

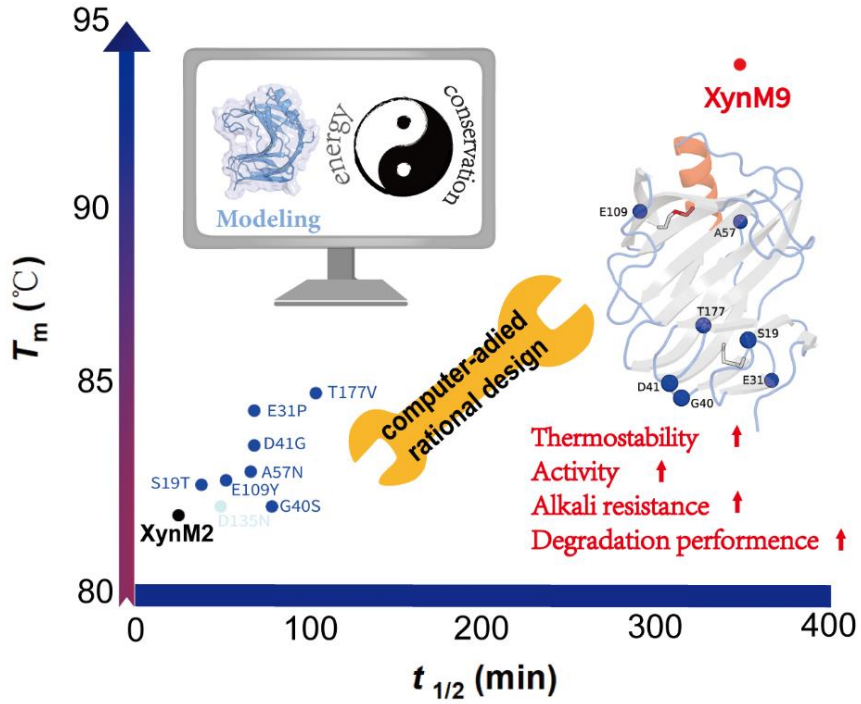

Through computer-aided rational design, our enhanced xylanase facilitates more sustainable lignocellulose degradation, reducing reliance on chlorine-based chemicals in paper bleaching.